



University of
Massachusetts
Amherst

Local Nanomechanical Variations of Cold-sprayed Tantalum Coatings

Item Type	Thesis (Open Access)
Authors	Chowdhury, Dhrubajyoti
DOI	10.7275/28611911
Rights	Attribution 4.0 International
Download date	2026-04-10 23:44:08
Item License	http://creativecommons.org/licenses/by/4.0/
Link to Item	https://hdl.handle.net/20.500.14394/32849

Local nanomechanical variations of cold-sprayed Tantalum coatings

A Thesis Presented

by

Dhrubajyoti Chowdhury

Submitted to the Graduate School of the
University of Massachusetts Amherst in partial fulfillment
of the requirements for the degree of

MASTER OF SCIENCE IN MECHANICAL ENGINEERING

MAY 2022

Department of Mechanical and Industrial Engineering

**LOCAL NANOMECHANICAL VARIATIONS OF COLD-SPRAYED
TANTALUM COATINGS**

A Thesis Presented

by

DHRUBAJYOTI CHOWDHURY

Approved as to style and content by:

Stephen S. Nonnenmann, Chairperson

Wen Chen, Member

Jae-Hwang Lee, Member

Sundar Krishnamurty, Department Head
Mechanical & Industrial Engineering Department

DEDICATION

To my paternal and maternal grandparents,

Late Sudhanshu Mohan Chowdhury

Late Lila Chowdhury

Syama Prosad Sengupta

Late Bubul Sengupta

ACKNOWLEDGMENTS

I would like to thank my advisor Professor Stephen S. Nonnenmann for his support and guidance throughout my journey as a Master's student. His kind and motivating words helped me to learn and the invaluable discussions during our meetings were a rich source of development of my own as well as for my research. I do extend my thanks to Professor Wen Chen and Professor Jae-Hwang Lee, my thesis committee members also for their encouragement and suggestions to my thesis. I am also thankful to Professor Michael J. Jercinovic from the Department of Geosciences for helping us with EPMA studies, which played a pivotal role in my research. I would also extend my gratitude to Army Research Lab and Solvus Global for supplying the samples for my research.

I also extend my thanks to my colleague, Jieun Park for training me on the Atomic force microscope. My other colleagues from our laboratory also supported, encouraged and motivated me during my research.

I am grateful to my uncle, aunt and cousin living in the Worcester area for showering me with love and affection during my stay at Amherst. Lastly, I am thankful to my parents for their love, encouragement, support and affection!

ABSTRACT

Local nanomechanical variations of cold-sprayed Tantalum coatings

MAY, 2022

DHRUBAJYOTI CHOWDHURY, B.Tech, SRM INSTITUTE OF SCIENCE AND TECHNOLOGY, KATTANKULATHUR, INDIA

M.S.M.E., UNIVERSITY OF MASSACHUSETTS AMHERST

Directed by: Professor Stephen S. Nonnenmann

Cold spray (CS) deposition of metals is a process involving deposition of materials in the solid or semi-solid state. It also has lower operating temperatures, and oxidation is greatly reduced in the process. The process is beneficial for refractory metals, such as tantalum, which are tough and difficult to machine. The interface between the CS powder and the substrate is the most important region for the study of mechanical properties as it is where the bonding process occurs first; studying mechanical properties at the nanoscale will give us a better idea of the mechanical properties of the coated surface. The present work investigates multiple-sprayed conventional and low-hydrogen treated tantalum powders on stainless steel substrates and also single-sprayed nitrogen-treated tantalum powders on aluminum substrate using Atomic force microscopy (AFM). It also discusses the effects of topography on the local changes in modulus.

AFM is an instrument that measures the site-specific property of the sample. In this work, the local Young's modulus is studied using force-distance curves. Calibration of the AFM cantilever and the photodetector used to measure the cantilever, is a vital step before the actual process. The conventional method of calibration can cause damage to the tip as

it arbitrarily penetrates into the sample creating a cantilever deflection vs. tip penetration curve, giving the sensitivity of the photodetector.

AFM is highly dependent on topographical features as the cantilever tip-sample interaction can vary, causing variations in the property mapped. This work, however uses a non-contact method of calibration which saves the cantilever tip from potential damages, saving the results from the detrimental effects of tip topography. The work also discusses the effects of local sample deformation and volume of tip-surface contact on local changes in Young's modulus at the interface of coating and substrate.

This work uses Electron micro-probe analysis (EPMA) to show the presence of oxides at the interface. The presence of oxides changes the bond energy as compared to a pure tantalum bond, ultimately affecting the local modulus mapped using AFM. The effect of oxides on the local modulus at the coating-substrate interface is theoretically discussed.

TABLE OF CONTENTS

	Page
ACKNOWLEDGMENTS	iv
ABSTRACT	v
LIST OF FIGURES	x
LIST OF SYMBOLS AND ABBREVIATIONS.....	xiii
CHAPTER	
1. INTRODUCTION	1
1.1 Cold spray	1
1.1.1 History of CS	1
1.1.2 Comparison with traditional thermal spray coating techniques	2
1.1.2.1 Advantages of CS over thermal spray techniques	2
1.1.2.2 Disadvantages of CS over thermal spray techniques	4
1.1.3 Factors affecting CS coatings	4
1.1.3.1 Spray powder deformation behavior	4
1.1.3.2 Spray gun parameters	6
1.1.3.2.1 Spray angle	6
1.1.3.2.2 Standoff distance	6
1.1.3.3 Spray particle velocity	7
1.1.4 CS of refractory metals	8
1.1.5 Applications of CS	9
1.2. Atomic force microscopy	10
1.2.1 Advantages and disadvantages of AFM	12
1.2.2 Classification of AFM	12
1.2.2.1 Contact mode AFM	13
1.2.2.2 Intermittent mode AFM	13
1.2.2.3 Non-contact mode AFM	13
1.2.3 Contact mechanics models used for AFM study	14
1.2.3.1 Hertz contact mechanics model	14
1.2.3.2 Sneddon's contact mechanics model	15
1.2.4 Need for calibrating the AFM cantilever	16

1.2.5 Characterization using AFM	16
1.2.6 Comparison with nanoindentation techniques	18
2. MOTIVATION AND RESEARCH STATEMENT	19
2.1 CS of refractory metals	19
2.2 Oxide content of CS coatings	19
2.3 Nanomechanical variations due to tip and sample topography	20
2.4 Research statement	21
3. MEASUREMENT OF LOCAL NANOMECHANICAL PROPERTIES USING ATOMIC FORCE MICROSCOPY (AFM): MECHANISM AND METHODOLOGIES	23
3.1 Contact-based calibration method: Using cantilever deflection vs. tip penetration curve mapped on a hard sample	24
3.2 Non-contact based calibration method: Using thermal noise spectrum.....	25
4. SAMPLE DESCRIPTIONS	27
4.1 Multi-spray samples	27
4.1.1 Tantalum powder-stainless steel substrate sample (Ta-SS).....	27
4.1.2 Low hydrogen treated Tantalum powder-stainless steel sample (LTa- SS)	27
4.2 Single-spray sample	28
5. LOCAL VARIATIONS IN YOUNG'S MODULUS DUE TO TOPOGRAPHIC AND OXIDATION CHANGES	29
5.1 Topographic changes	29
5.1.1 Background and motivation	29
5.1.2 Variations due to tip wear	29
5.1.3 Variations due to volume of the surface touched by the tip	30
5.1.4 Variations due to sample particle deformation at the point of contact of the tip and sample	30
5.1.5 Images obtained via AFM	31
5.1.5.1 AFM tip calibration	31
5.1.5.2 Interpretation of the images	31
5.2 Oxidation changes	34
5.2.1 Background and motivation	34
5.2.2 Electron micro-probe analysis (EPMA) of Tantalum-stainless steel cross-section samples	36
5.2.3 Local modulus mapping using AFM	36

6. CONCLUSIONS	37
7. FUTURE WORK	39
8. BIBLIOGRAPHY	41

LIST OF FIGURES

Figure	Page
1. Cold spray coating setup.....	1
2. Development of the CS process.....	2
3. Typical illustration of molten spray particles attaching to the substrate in thermal spray technology.....	2
4. Gas temperature comparison of thermal spray techniques and CS.....	3
5. Schematic representation of oxide and porosity formation in thermally sprayed coatings.....	3
6. Comparison of two copper coatings produced from the same feedstock powder	
(a) copper-plasma in ambient air with ~5% porosity and 1.7% wt. oxide.....	4
(b) copper sold-sprayed in ambient air with <1% porosity and only 0.3% wt. oxide.....	4
7. Simulation of impact	
(a) Al on Al at 775m/s (soft on soft).....	5
(b) Ti on Ti at 865m/s (hard on hard).....	5
(c) Al on mild steel at 365m/s (soft on hard).....	5
(d) Ti on Al at 655m/s (hard on soft).....	5
8. Minimum diameter required for adiabatic shear instability.....	5
9. (a) Effect of spray angle on the relative deposition efficiency of copper (inset) spray gun arrangement with respect to the substrate and its change in angle along horizontal direction.....	6
(b) effect of spray angle on coating porosity.....	6
10. Effect of standoff distance on relative deposition efficiency of aluminium, titanium and copper powders.....	7
11. Change in the level of porosity with respect to standoff distance.....	7
12. Influence of particle velocity on deposition efficiency (inset) influence of spray conditions and particle diameter on particle velocity.....	8
13. Schematic diagram of an atomic force microscope, (inset) tip which is brought close to the sample (both represented in the form of atoms).....	10
14. Schematic diagram of a typical force-distance curve, (inset) shows the tip-cantilever assembly movements when it approaches and retracts from the sample.....	11

15. Different modes of AFM operation.....	13
16. Hertzian contact mechanics model with a spherical indenter of radius R.....	15
17. Sneddon’s model with conical indenter.....	15
18. Angle of the AFM cantilever.....	16
19. Mo(C)N coatings at 7.1% C	
(a) using SEM at x5000 magnification.....	17
(b) corresponding 3D image of the same sample using AFM scanning area 40 X 40 μm.....	17
20. (a) Young's modulus mapping using bimodal AFM of an LDPE sample. The dotted line shows the profile along which the Young's modulus indicated in the lower graph varies.....	17
(b) mapping of Ti/Si metals using bimodal tapping mode in AFM.....	17
21. Oxygen content in different warm sprayed (WS) and cold sprayed (CS) coatings.....	20
22. Force mapping process during nanomechanical property measurement using tip- sample interaction properties, (inset) tip-sample interaction at each point, shown by blue lines in the actual image.....	21
23. Representation of the AFM mapping process.....	24
24. Variation in cantilever deflection according to sample topography.....	24
25. Deflection vs. tip penetration for a quartz sample.....	25
26. Thermal noise spectrum of an AFM cantilever.....	25
27. Graphical depiction of multiple pass cold-spray process.....	27
28. Graphical representation of Tantalum-stainless steel samples	
(a) top cross-section.....	27
(b) vertical cross-section.....	27
29. (a) Graphical representation of single-sprayed coating	28
(b) interface region investigated.....	28
30. Process of mapping of local Young's modulus.....	29
31. Difference in topography mapped due to tip wear.....	30

32. Improper volume of contact of tip and sample.....	30
33. (a) Topography.....	31
(b) local Young's modulus variations of Ta-SS vertical cross-section samples (black line shows the interface between coating and substrate).....	31
34. (a) Topography.....	31
(b) local Young's modulus variation of LTa-SS vertical cross-section samples (white line in (a) and black line in (b) shows the interface of coating with substrate).....	31
35. (a) Topography.....	32
(b) Young's modulus variations in Ta-SS top interface (white line in (a) and black line in (b) indicates the interface between coating and substrate).....	32
36. (a) Topography.....	32
(b) Young's modulus variations in LTa-SS top interface (white line shows the interface between coating and substrate).....	32
37. (a) Topography.....	32
(b) Young's modulus variations in Ta-Al sample (white line in (a) and black line in (b) shows the interface).....	32
38. (a) Local modulus variation.....	33
(b), (c) force-distance curves indicating local particle deformation of LTa-SS top section sample.....	33
39. Schematic diagram of particle impact and bonding at the interface of sprayed particle and substrate interface.....	34
40. (a) Bond between Tantalum atoms.....	35
(b) red lines show different bonds due to the presence of oxygen atoms.....	35
41. EPMA study showing oxide content at the coating-substrate interface.....	35
(a) Ta-SS.....	35
(b) LTa-SS vertical cross-section samples.....	35
42. Local modulus changes along the interface of LTa-SS (black lines) can be due to the presence of oxides.....	36

LIST OF SYMBOLS AND ABBREVIATIONS

CS	Cold-spray
AFM	Atomic force microscopy
WS	Warm-spray
E	Young's modulus
h	Indentation depth
R	Tip radius
ν	Poisson's ratio
P	Applied load
F	Force applied
δ	Sample deformation
α	Coefficient
β	Coefficient
E_{eff}	Effective Young's modulus

CHAPTER 1

INTRODUCTION

1.1 Cold spray

The cold spray (CS) process is a method of impacting and attaching powdered particles to a suitable substrate. The powdered particles are accelerated to high velocities using suitable gases through a nozzle of specific designs. Eventually, the particles are deformed on the substrate and are bonded to it. The term "cold spray" has been used due to the low temperature (-100 to 100°C) of the expanded stream of gas that exits the nozzle. Figure 1 shows a typical cold spray coating setup.

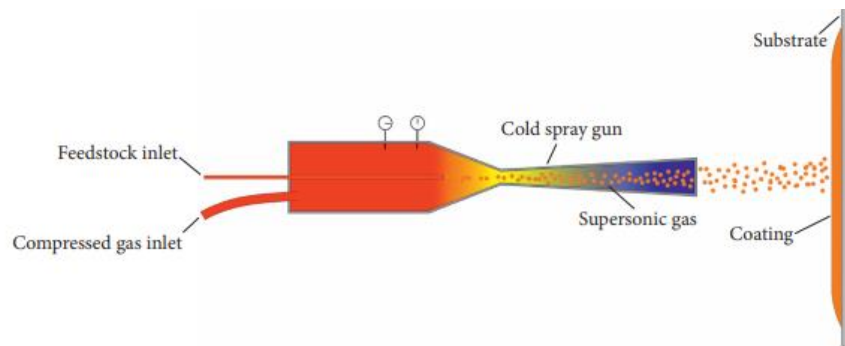


Figure 1: Cold spray coating setup[1]

1.1.1 History of CS

CS is a recently emerged technology in the field of thermal spray technology and was developed in the mid-1980s by A. Papyrin and his team at the Institute of Theoretical and Applied Mechanics of the Siberian Branch, now called Khristianovich Institute of Theoretical and Applied Mechanics in Novosibirsk city, Russia. While studying aerodynamic systems in a supersonic wind tunnel, these researchers decided to use small particles of steel and aluminum mixture with the supersonic gas system to make a two-phase (gas + solid) fluid. It was observed that particles of different sizes and sprayed at

different velocities and angles were deposited onto the material surface when the fluid velocity had reached a certain critical value. This new process is termed as "cold spray" [2], [3]. Figure 2 shows a historic development of the CS process.

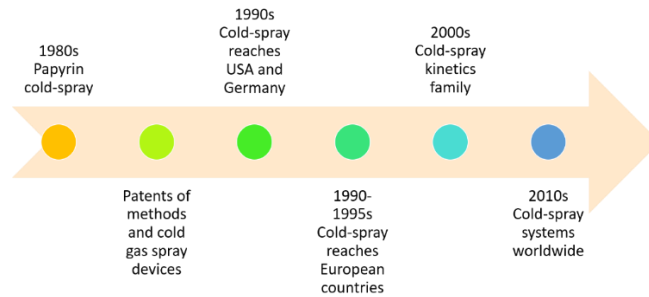


Figure 2: Development of the CS process (adapted from [3])

1.1.2 Comparison with traditional thermal spray coating techniques

"Thermal spray" is a term used to describe a broad family of technologies such as arc spray, plasma spray, flame spray, and high-velocity oxy-fuel spray (HVOF). Typically, it involves melting metal particles to be coated into droplets and spraying them on the substrate. The droplet spreads on the substrate and cools at specific cooling rates (Figure 3).

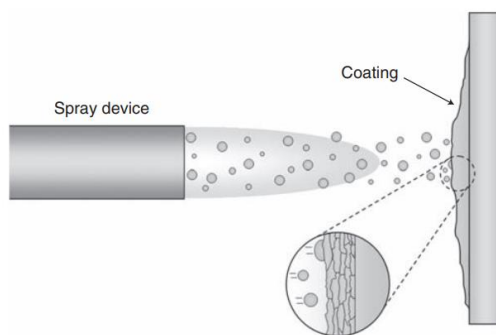


Figure 3: Typical illustration of molten spray particles attaching to the substrate in thermal spray technology[4]

1.1.2.1 Advantages of CS over thermal spray techniques

As indicated in Figure 4, CS techniques have a lower operating temperature as compared to thermal spray techniques. Due to this reason porosity and oxide formation

can be reduced in CS techniques. However, there can be traces of oxides in CS coatings, which are

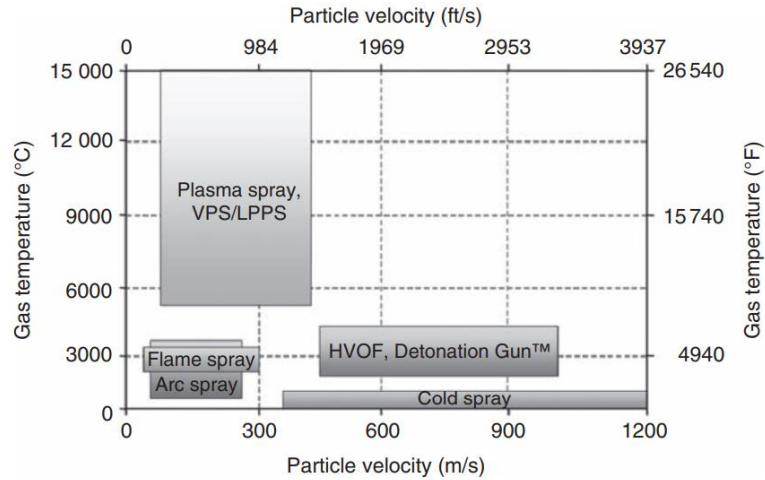


Figure 4: Gas temperature comparison of thermal spray techniques and CS[4]

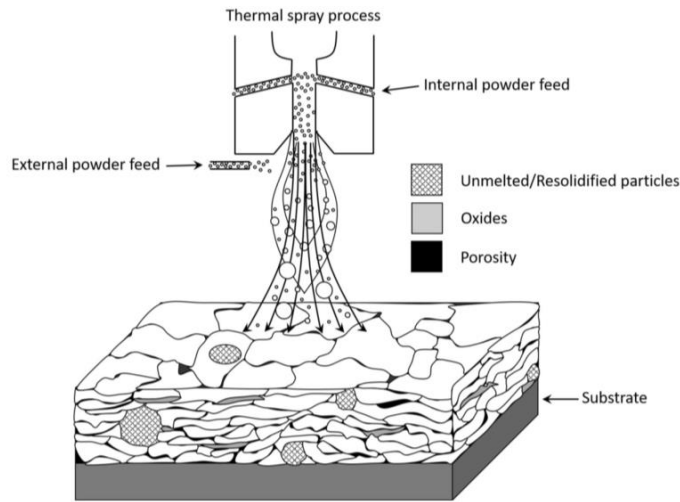


Figure 5: Schematic representation of oxide and porosity formation in thermally sprayed coatings[5]

discussed in later sections. The significantly reduced porosity results from the absence of splashing and its solid-state impacting nature supports its ability to have lower levels of porosity. As the metals are deposited on a molten or semi-molten state on the substrate, there is an increased chance of oxide formation on the coating unlike in CS where the metals are not molten and is impinged in the solid state. Figures 5 and 6 supports a demonstration

of these phenomena. Due to the solid – state attachment nature of CS, it mostly maintains the initial phases, unlike thermal spray techniques. Also, CS does not experience much grain growth, unlike thermal spray techniques.

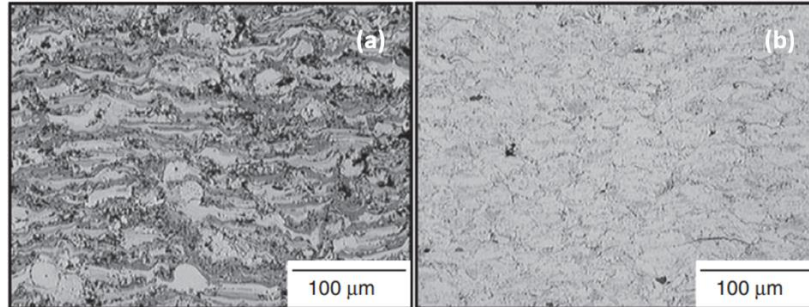


Figure 6: Comparison of two copper coatings produced from the same feedstock powder (a) copper plasma-sprayed in ambient air with ~5% porosity and 1.7% wt. oxide (b) copper cold sprayed in ambient air with <1% porosity and only 0.3% wt. oxide[4]

1.1.2.2 Disadvantages of CS over thermal spray techniques

Unlike thermally sprayed techniques, which can deposit a wide-range of materials such as metals, polymers, and ceramics, CS can only deposit ductile materials and hence mostly ductile metals. The most accepted mechanism for CS is adiabatic shear instability plastically deforms sprayed metal powders onto the substrate, which are eventually attached to them. This demands high ductility for the powders.

Also, CS processes generally require more quantities of process gas and in many cases must rely on hydrogen as the process gas. This makes this process expensive in most cases compared to thermal spray technologies[4].

1.1.3 Factors affecting CS coatings

1.1.3.1 Spray powder deformation behavior

The most accepted mechanism of bonding in CS processes is adiabatic shear instability. "Adiabatic" refers to the absence of heat transfer, and in this case, the heat generated due

to impact remains on the surface. It requires high strain deformation of the sprayed particles, and thus high ductility is a requirement for the spray particles.

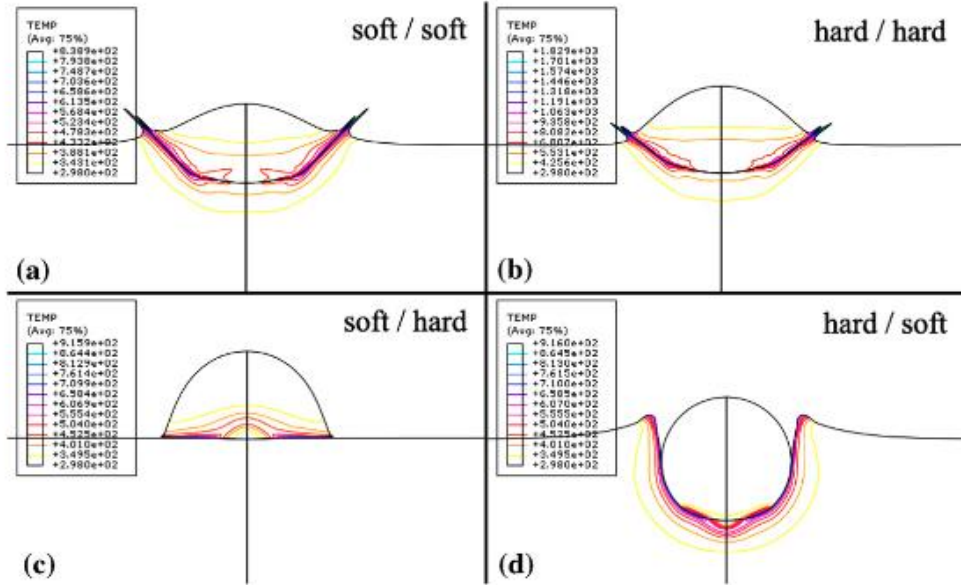


Figure 7: Simulation of impact (a) Al on Al at 775m/s (soft on soft) (b) Ti on Ti at 865 m/s (hard on hard) (c) Al on mid steel at 365 m/s (soft on hard) (d) Ti on Al at 655m/s (hard on soft)[6]

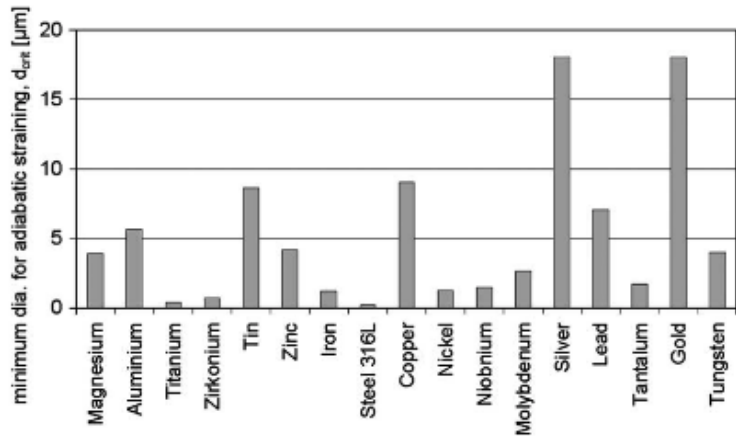


Figure 8: Minimum diameter required for adiabatic shear instability[7]

The high kinetic energy generated during this process creates high pressure that promotes bonding[6–9]. Walker et al.[6] also studied the bonding mechanism of CS coatings and classified four categories on the basis of hardness of both the powder and the substrate (Figure 7). Figure 8 shows the minimum powder diameter required for adiabatic shear instability to occur for different metals.

1.1.3.2 Spray gun parameters

1.1.3.2.1 Spray angle

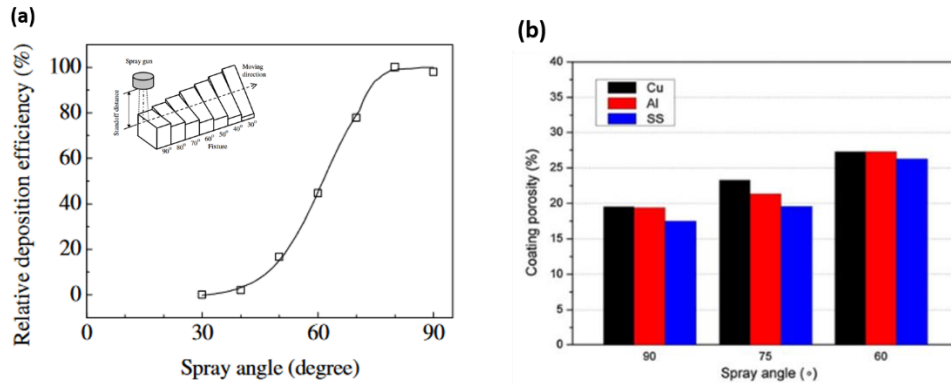


Figure 9: (a) Effect of spray angle on the relative deposition efficiency of copper (inset spray gun arrangement with respect to the substrate and its change in angle along horizontal direction [10], (b) effect of spray angle on coating porosity[11]

Li et al.[10] pointed out that the normal component of particle impact velocity changes with spray angle. They have studied the effect of the change in spray angle for copper and titanium particles while the spray angle was continuously changed during the spray process. They have found that relative deposition efficiency for both copper and titanium particles change with change in spray angle and is highest for 90° (Figure 9).

Yin et al.[11] studied the effects of spray angle in CS titanium particles on aluminium, copper, and stainless steel substrates. They have found that porosity of the coating changes with spray angle and the least porosity is observed in the case of 90° spray angle (Figure 9(b)).

1.1.3.2.2 Standoff distance

Li et al.[12] studied the effects of distance between spray gun tip and the substrate, which is commonly known as standoff distance. They have studied aluminium, copper and

titanium powders and have found the effect of standoff distance on relative deposition efficiency (Figure 10).

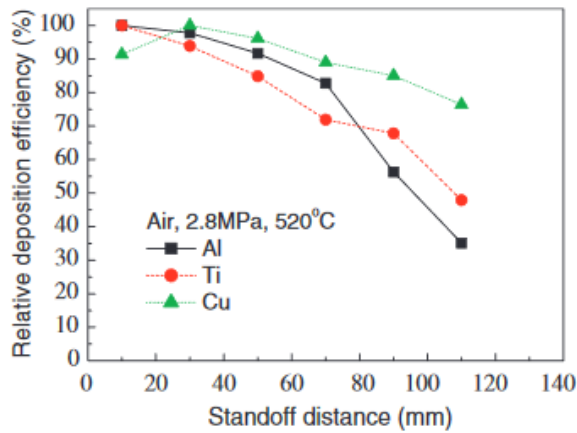


Figure 10: Effect of standoff distance on relative deposition efficiency of aluminium, titanium and copper powders[12]

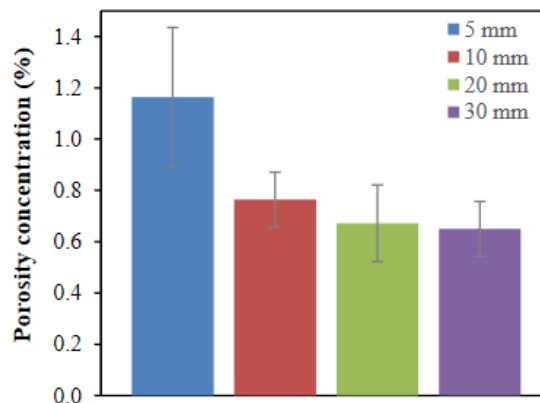


Figure 11: Change in the level of porosity with respect to standoff distance[13]

Cetin et al.[13] also studied the effects of copper cold sprayed powders and studied the effects of porosity with respect to standoff distance. Porosity decreased with increase in standoff distance (Figure 11).

1.1.3.3 Spray particle velocity

The spray particles are released from the spray gun nozzle with a certain velocity. It has been found that it should attain a certain value for effective bonding. This value of velocity is termed as "critical velocity". In case the velocity is less than the "critical velocity", a

phenomenon similar to grit blasting can cause surface abrasion. As shown in Figure 12, particle velocity is dependent on spray conditions and particles diameter and has its influence on deposition efficiency[6].

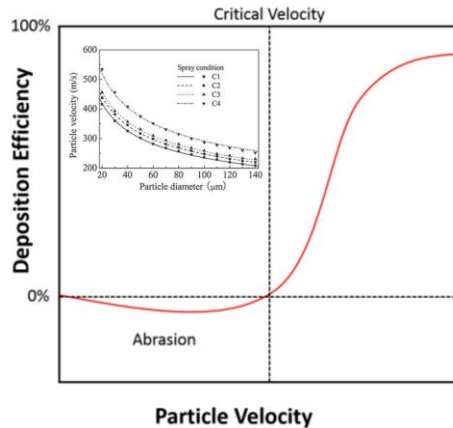


Figure 12: Influence of particle velocity on deposition efficiency (inset) influence of spray conditions and particle diameter on particle velocity [6]

1.1.4 CS of refractory metals

Refractory metals are a class of metals with a very high melting point and good wear resistance. Due to their high melting point temperature, they are primary candidates for applications related to high-temperature nuclear applications. However, there is a limitation in their application due to difficulty in their fabrication[14]. They are typically fabricated by powder processing methods[15].

The high strength and toughness of refractory metals limits their manufacturing ability using conventional methods such as machining or extrusion. Powder metallurgy serves as an efficient method of manufacturing of these alloys due to its low-temperature requirement. Therefore, CS suits the purpose of manufacturing due to its nature of impact-mediated sintering[16].

1.1.5 Applications of CS

CS is a recently developed technique with the potential of additively manufactured components and also to repair damaged components[17]. They have their uses in thermal power plants where the sprayed coatings provide protection against failures such as erosion, corrosion, and high-temperature oxidation. High adhesion strength and hardness along with retention of most of the original powder properties, gives this technique an advantage in nuclear power plant sectors as well[18].

Ševeček et al.[19] used CS to deposit chromium powders as fuel cladding which had enhanced properties compared to the traditional Zr-based alloys. The chromium coating exhibited good bond strength and corrosion resistance even with the absence of post-fabrication surface treatments. According to the authors, the CS technique has its advantage in terms of high deposition efficiency and advantage for the industries. It, however, resulted in a nonuniform and heterogeneous structure.

Widener et al.[20] discussed the economic aspects of repair using CS technology. As the technology has the ability to repair a part using spraying instead of replacing it, there is cost and environmental benefit. The authors have described the process as "green technology" and have also mentioned its use in long-term sustainability of high-value assets.

Barnett et al.[16] used cold sprayed refractory metals in gun barrel liners for chrome reduction. As per the investigation, successful cladding makes CS process as an alternative

to extrusion for refractory donor tubes (the extrusion process for refractory metals can be difficult and expensive).

Champagne et al.[21] provides a comprehensive review of the application of CS techniques in the field of aerospace engineering. According to the authors, the process can deposit aluminium and its alloys to protect of magnesium components against corrosion. The method can also be used for wear protection around fastener holes and protecting hydraulic tubes against chafing. Apart from aerospace applications, the authors have also investigated that CS can be used to join dissimilar metals such as ZE41A-T5 Mg and 6061 Al with bond strength equal or superior to the substrate.

1.2. Atomic force microscopy

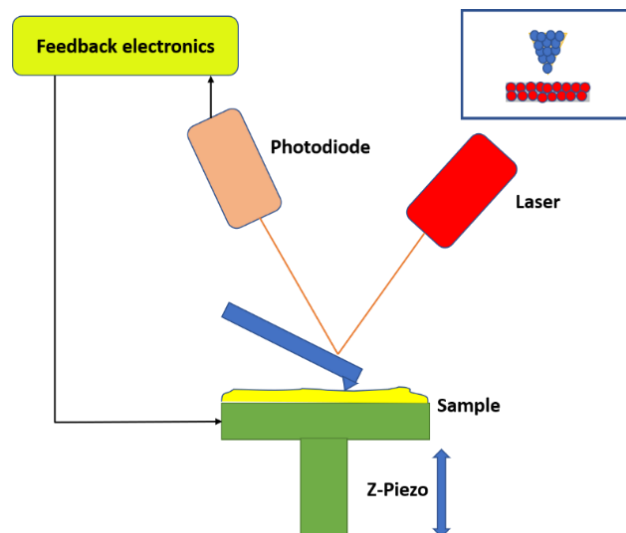


Figure 13: Schematic diagram of an atomic force microscope, (inset) tip which is brought close to the sample (both represented in the form of atoms)

Atomic force microscopy (AFM) was invented in 1986[22], [23] representing a method that measures the force acting between a fine tip and the sample and has its applications in

materials science, life science, polymer science, biotechnology, biophysics, and nanotechnology[24]. Figure 13 shows the typical arrangement of an AFM setup.

The tip is brought close to the sample, such that it causes bending of the cantilever and tip assembly due to the interatomic force (inset). The maximum permissible force and deflection of the cantilever is specified at the beginning of the experiment (it is called Set Point). The laser sets out light rays which are reflected from the cantilever and received by the photodetector.

At a certain atomic position in the sample, the tip is brought close to the sample such that it causes a deflection in the cantilever. This deflection is recorded by the photodetector using the laser ray reflected from the bent cantilever. It then compares this deflection with the Set Point and sent one signal to the Z-piezo deflection of the cantilever due to change the position such that it matches the Set Point. Another signal is sent to the computer, which records information in the form of image maps using the deflection of the cantilever. This process is repeated in an area within the sample as specified by the user.

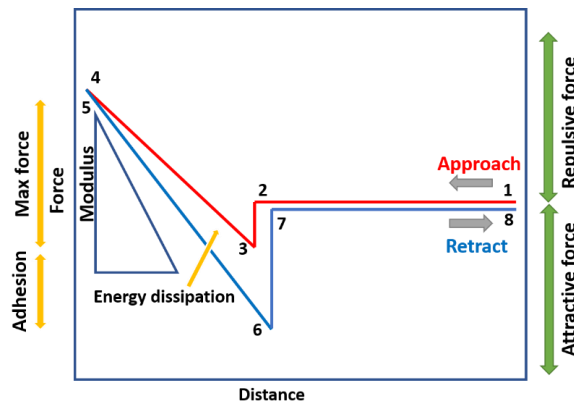


Figure 14: Schematic diagram of a typical force-distance curve, (inset) shows the tip-cantilever assembly movements when it approaches and retracts from the sample

Figure 14 shows a schematic representation of a force-distance curve. During the approach action, the tip is brought close to the sample such that no atomic forces come into action (steps 1-2). Once the tip is brought too close to the sample, it initially experiences an attraction from the atoms of the sample (steps 2-3). The tip atoms face repulsion from atoms of the sample such that it reaches to a peak repulsion force (step 3-4). It then begins the retraction action.

During the retraction action, the tip once again faces attraction from the sample and it reaches to a peak attractive force (step 5-6). It again faces repulsion from the sample atoms and it once again reaches back to its initial position (steps 6-8). The slope of the linear section of the line during steps 5-6 gives the Young's modulus of the sample, which is the primary mechanical property studied in this work.

1.2.1 Advantages and disadvantages of AFM

Atomic force microscopy can measure samples at the molecular as well as the atomic level. It also does not have to be carried out in extreme conditions. Its major advantage lies in its versatility in measuring various samples like polymers, metallic nanoparticles, ceramics, human cells and also individual molecules of a DNA[25].

The main disadvantage of the AFM process is its ability only to obtain surface information from the sample. Also, due to the nature of AFM probes, they cannot measure steep walls or overhangs[26].

1.2.2 Classification of AFM

An important way to classify AFM is on the basis of their modes of operation. Figure 15 shows the different modes of operation.

1.2.2.1 Contact mode AFM

In this mode, the cantilever is dragged across the surface and cantilever deflection is used to measure surface contours directly. The force between the tip and the surface is kept constant during scanning by maintaining a constant deflection. The tip is constantly adjusted to maintain constant deflection and this is shown as data. This method can be used for hard metals but cannot be used for soft surfaces as it can deform them[27], [28].

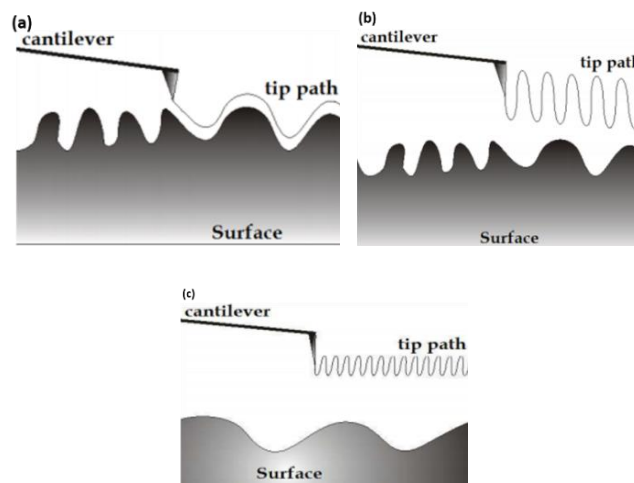


Figure 15: Different modes of AFM operation [27]

1.2.2.2 Intermittent mode AFM

It is similar to the contact mode; however, the cantilever makes intermittent contact with the surface and lightly taps it at a resonant frequency. Due to the small contact time, lateral forces are reduced dramatically. This mode is suitable for structures weakly bound to the surface and also for soft surfaces[27].

1.2.2.3 Non – contact mode AFM

In this mode the probe does not touch the sample but oscillates above it during scanning at a frequency close to its fundamental frequency. Phase, resonance, and amplitude of

oscillation are modified by tip-sample interaction forces. These oscillation changes with respect to reference oscillation provide information about the sample's surface characteristics[27], [28].

1.2.3 Contact mechanics models used for AFM study

The data processing in AFM is done on the basis of contact mechanics models. The differences in Young's modulus can be as significant as 30% in the case of different contact mechanics models. Hence, it is essential to choose the appropriate contact mechanics model for the sample to be studied[29].

1.2.3.1 Hertz contact mechanics model

It is widely used in AFM studies and is used when there is a spherical tip. If indentation depth (h) is smaller than tip radius (R) then the loaded data can be fitted in the given equation:

$$P = \frac{4}{3} \frac{E}{1-\nu^2} R^{1/2} h^{3/2} \quad (1)$$

Here E , ν are Young's modulus and Poisson's ratio of the sample respectively. P is the applied load. Young's modulus can be easily calculated as the fitting parameter provided that indenter dimensions and Poisson's ratio of the sample are known.

However, the following conditions must be met in order to use the Hertzian contact mechanics model:

- (a) Sample should be homogeneous.
- (b) Sample should be isotropic.
- (c) There should be a linear elastic response in the sample.

Biological samples do not fit into these conditions and hence this contact mechanics model cannot be used for them. It has also been investigated that the Hertzian response can be purely used for elastic responses and samples having low h/R ratios[29]. Figure 16 provides the representation of the Hertzian contact mechanics model.



Figure 16: Hertzian mechanics model with a spherical indenter of radius R [30]

1.2.3.2 Sneddon's contact mechanics model

It is another contact mechanics model which is based on the following assumptions[31]:

- (a) Deformation in the elastic regime
- (b) Deformation small with respect to the radius of the projected contact area
- (c) Force applied is perpendicular to the surface (shear force is absent)
- (d) Semi-infinite sample



Figure 17: Sneddon's model with conical indenter[30]

The following formula relates the force applied (F) to the Young's modulus mapped

(E_{eff})[32] :

$$F = \alpha E_{eff} \delta^\beta \quad (2)$$

Here δ is the sample deformation, α is a coefficient that depends on the tip's geometry and size and β is a coefficient only dependent on tip's geometry. Figure 17 is a representation of this model.

1.2.4 Need for calibrating the AFM cantilever

It is to be noted that the stiffness of the cantilevers can vary due to the variation in the angle in which they are manufactured (Figure 18). This angle has an influence on the force which is to be applied. Hence, the proper measurement of the AFM cantilever's stiffness is essential in achieving accuracy in force measurements.

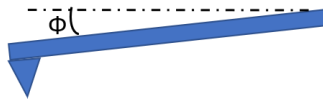


Figure 18: Angle of AFM cantilever

Also, the photodetector turns the cantilever deflection into volts and gives the output. The sensitivity (amount of photodiode response per unit cantilever deflection) has also to be determined. This gives the need for calibration of the AFM cantilever and the photodiode [33,34]. The details of the calibrated processes used for this study are elaborated in chapter 3.

1.2.5 Characterization using AFM

Kuznetsova et al.[35] investigated topography of Mo(C)N coatings using AFM which also helped in detecting heterogeneity of the surface. They have detected the variation of tribological properties using different phases and surface characterizations studied using AFM. Figure 19 shows the Scanning electron microscopy (SEM) image and its corresponding 3D topography mapped using AFM.

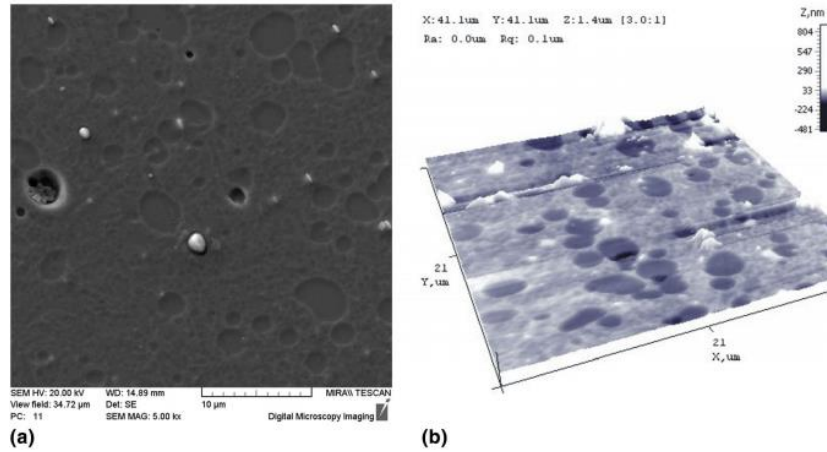


Figure 19: Mo(C)N coatings at 7.1% C (a) using SEM at x5000 magnification (b) corresponding 3D image of the same sample using AFM scanning area 40 X 40 μm[35]

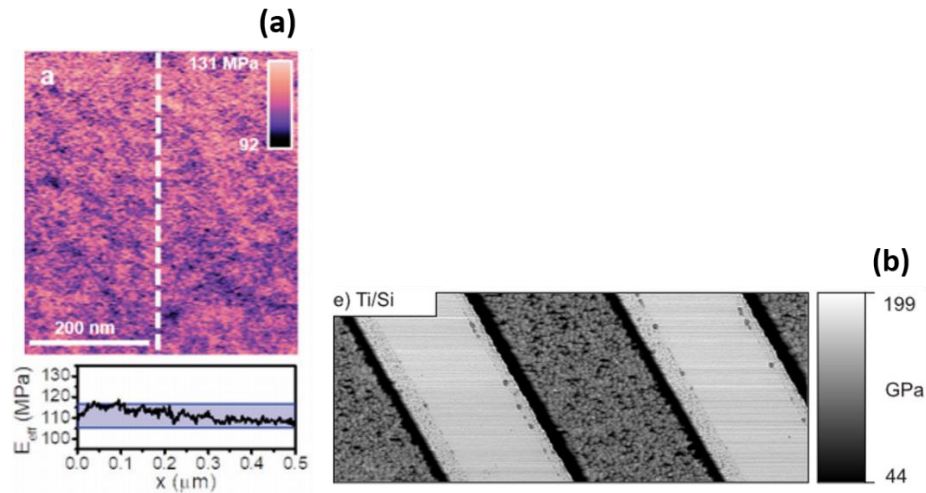


Figure 20: (a) Young's modulus mapping using bimodal AFM of an LDPE sample. The dotted line shows the profile along which the Young's modulus indicated in the lower graph varies[36] (b) mapping of Ti/Si metals using bimodal tapping mode in AFM[37]

Benaglia et al.[36] provides an overview of a fast and high-resolution mapping technique of viscoelastic materials. It has elaborated on the use of AFM in the characterization of viscoelastic properties in its bimodal mode. Figure 20(a) shows the elastic modulus mapping of polyolefin elastomer (LDPE). It can also be seen from Figure 20(b) that AFM can also map metals such as titanium (Ti) and silicon (Si)[37]. Titanium also has refractory metal characteristics[38]. Thus, it can be inferred that AFM has the capacity to characterize a wide range of moduli.

1.2.6 Comparison with nanoindentation techniques

Kong et al. [39] concluded the following points with regards to indentation depth of AFM with nanoindentation:

1. AFM probe measurement is a non-destructive process.
2. Scale of detection is finer in case of AFM as it can detect individual points in a given area.

Thus, the second points mention the precision in the measurement of nanomechanical properties using AFM as compared to nanoindentation. With the use of AFM in the characterization of materials, there is a possibility of characterization of CS coatings. The use of AFM in mapping the topography as well as mechanical properties (such as Young's modulus) is beneficial in its use as an efficient characterization technique. AFM also has the ability to characterize a wide range of Young's modulus and it can also be seen those refractory metals such as titanium can be mapped. Thus, there lies a possibility of mapping tantalum using AFM techniques.

CHAPTER 2

MOTIVATION AND RESEARCH STATEMENT

2.1 CS of refractory metals

As mentioned earlier in section 1.4, conventional manufacturing techniques such as machining and extrusion can result in high costs and complications in fabrication. Powder metallurgy approaches such as CS are beneficial in the manufacturing of refractory metal-based components[16].

Tantalum (Ta) is a metal with high hardness and high melting point (2996°C), giving it the characteristics of a refractory metal. The following points highlights the benefits of cold spraying Ta powders instead of using conventional thermal spraying processes:

- (a) It requires high temperatures to melt and coat the samples.
- (b) It is reactive with gases such as oxygen, nitrogen and hydrogen at temperatures above 500°C and causes it to crack and lose its ductility[40].

2.2 Oxide content in CS coatings

Even though it was mentioned in section 1.2.1 that oxide formation could be reduced in CS coatings, further research has shown the presence of traces of oxides in these coatings. Kim et al.[41] has suggested the "impact-heating" induced in CS can form oxidation of the sprayed particles forming thin oxide films on the scale of nanometers. They have compared the microstructure of warm and cold sprayed Titanium coatings in order to find the oxide content in the coatings. Their coatings were produced using varied processing parameters. Figure 21 shows the oxygen content in the different coatings. The authors have also

predicted the influence of oxides on the bond formation and mechanical properties of the coatings.

Barnett et al.[16] suggested that Tungsten and Tantalum are sensitive to interstitial oxygen. Ductility of the deposit can be reduced, which cannot be regained even after heat-treatment. Cracking due to oxygen can also result due to the combined residual stresses in the feedstock. Thus, powders with oxygen content already present in them are also detrimental in terms of the coating properties. Li et al.[42] investigated that powder with low oxygen content required a low critical velocity of about 320 m/s. The critical velocity decreased with low oxygen content.

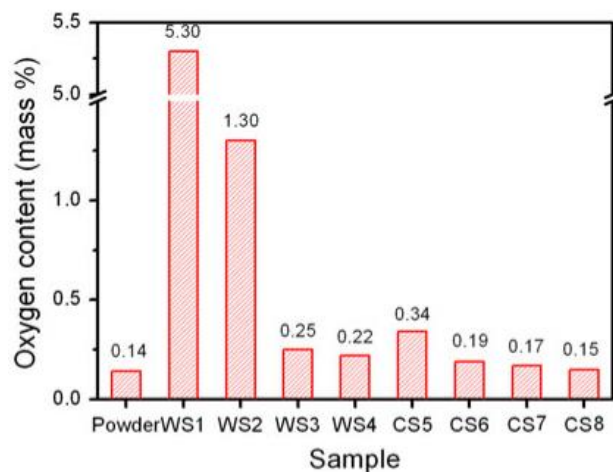


Figure 21: Oxygen content in different warm sprayed (WS) and cold sprayed (CS) coatings[41]

2.3 Nanomechanical variations due to tip and sample topography

Figure 22 shows schematically how the scanning process takes place in AFM. This is the conventional way of scanning which is studied in this work, where the tip interacts with the sample surface, and the interaction forces determine the nanomechanical properties at

each scan point. A scanning area is divided into segments, and the tip is brought to each of those segments, ultimately giving the nanomechanical map of the entire scan area.

The other way to map nanomechanical properties is by measuring the effect of the interaction force on some parameters related to the oscillation of the tip. However, this method is beyond the scope of this work [31].

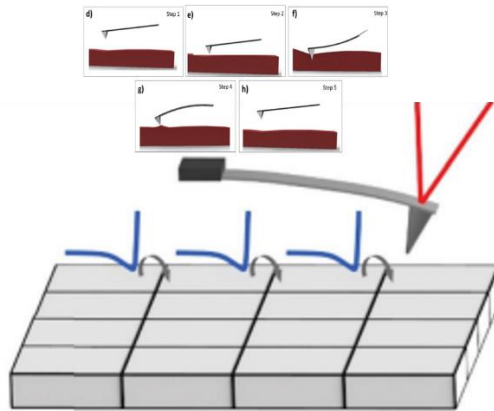


Figure 22: Force mapping process during nanomechanical property measurement using tip-sample interaction properties, (inset) tip-sample interaction [30] at each point, shown by blue lines in the actual image [31]

It is also to be noted that the evaluation of the mechanical properties at the nanoscale by the AFM is a site-specific process. The mechanics of the process involved during the tip and target sample interaction plays a key role in shaping the nanomechanical property mapped at that point [43].

2.4 Research statement

Nanomechanical mapping of cold-sprayed coatings using the data obtained using the force-distance curve mechanism used in AFM is reportedly less investigated. Bhushan [44] pointed out the importance of factors such as surface topography and surface properties in influencing the contact between two surfaces. The methodology used in this study uses

nanoscale mapping of mechanical properties using the force-distance curve obtained via the AFM tip and cold-sprayed sample interaction. Therefore, it is important to point out the various factors that play a key role in local changes of the nanomechanical properties.

CHAPTER 3

MEASUREMENT OF LOCAL NANOMECHANICAL PROPERTIES USING ATOMIC FORCE MICROSCOPY (AFM): MECHANISM AND METHODOLOGIES

The process in which a force-distance curve is plotted at every point in a given area is described in section 2. This is the method using which nanomechanical characterizations take place using the contact-mode AFM. Contact-mode AFM is studied in this work. Hertzian contact mechanics model is used as the governing model to map the nanomechanical characteristic of Young's modulus in this work with the assumptions as stated in section 2.3.1.

The need for calibration is mainly due to variations in the angle of the cantilever tip and also due to photodetector sensitivity variations as discussed in section 2.4. The user must have the calibrated stiffness of the cantilever (k_{app}) and the sensitivity of the photodetector, also known as Inverse optical lever sensitivity (InvoLS). The amount of deflection of the cantilever that occurred during this process is recorded by the instrument (Setpoint). At every point in the scan region, the feedback system signals the z-piezo to change its position to the setpoint once there is a deviation from it (Δz). The deviation occurs due to topography changes in the sample. The force as obtained post-calibration is given below [45]:

$$F = k_{app} \times \text{InvoLS} \times \Delta V \quad (1)$$

As per the Hertzian contact mechanics model, we can mention that the Young's modulus is a function of the force applied:

$$\text{Young's modulus} = f(\text{Force}) \quad (2)$$

Figure 23 schematically represents the process taking place during the mapping of Young's modulus by AFM. Figure 24 shows how the deflection of the cantilever varies according to the sample topography.

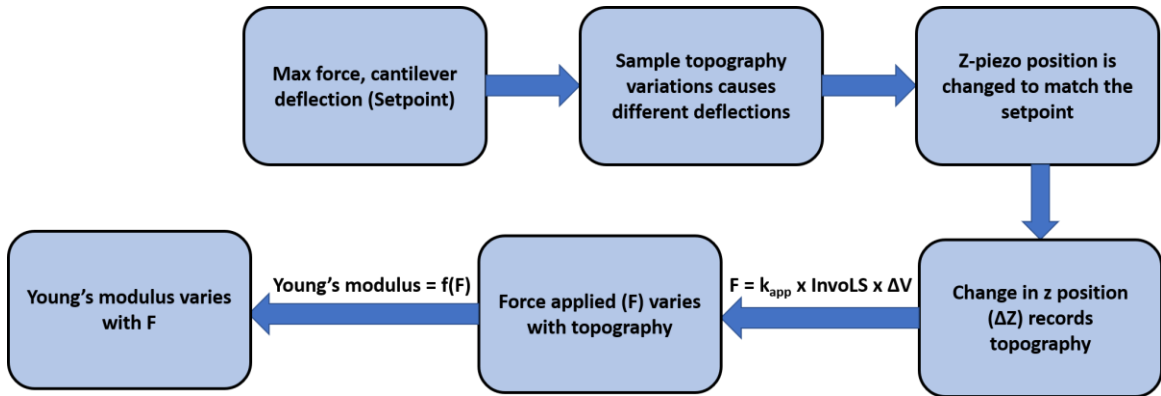


Figure 23: Representation of the AFM mapping process

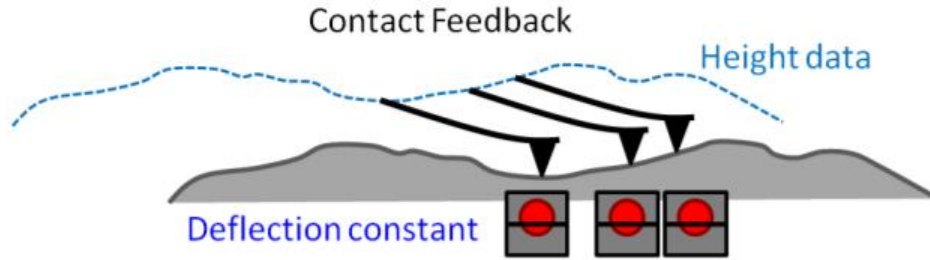


Figure 24: Variation in cantilever deflection according to sample topography [46]

3.1 Contact-based calibration method: Using cantilever deflection vs. tip penetration curve mapped on a hard sample

This is the most common method to calibrate a cantilever used for AFM and the photodetector sensitivity. A hard, non-deformable sample is used for this process. An arbitrary tip indentation distance is mentioned by the user. The cantilever deflection vs. tip penetration distance is calculated, and the inverse of its slope gives the InvoLS [45]. Figure 25 shows a curve obtained on a quartz sample.

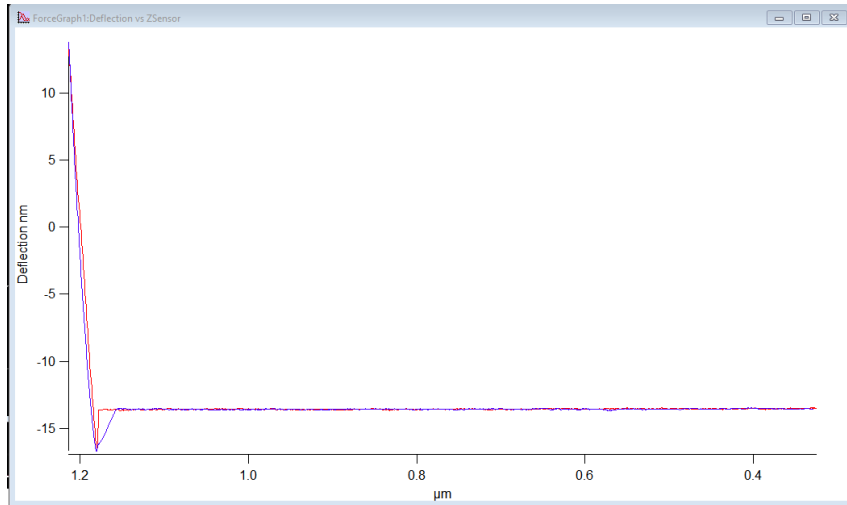


Figure 25: Deflection vs. tip penetration for a quartz sample

3.2 Non-contact based calibration method: Using thermal noise spectrum

The instrument used for this study has an in-built feature, "GetReal®" which calculates InvoLS using the thermal noise spectrum with cantilever dimensions and drive frequency as the governing parameters. It shows the resonant frequency as the peak and also calculates the calibrated stiffness of the cantilever (k_{app}). Figure 26 shows a sample thermal noise spectrum curve as obtained on the instrument.

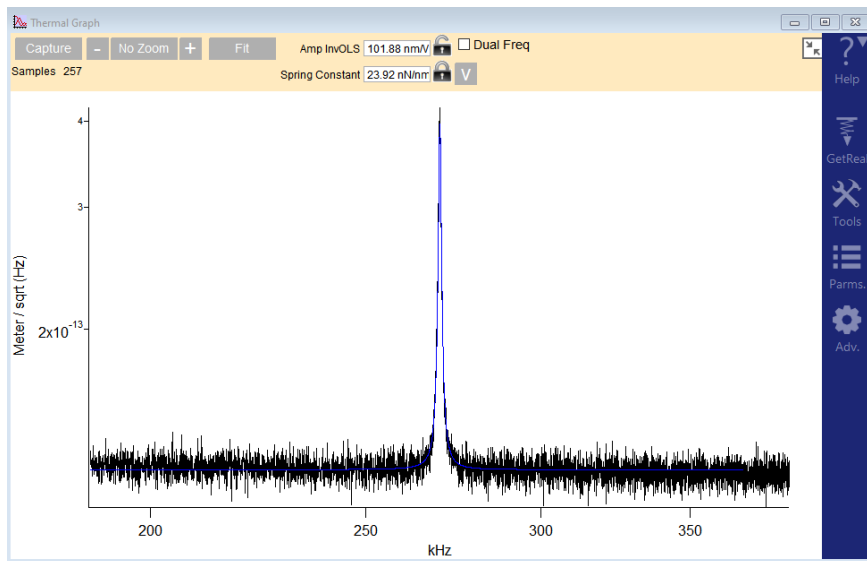


Figure 26: Thermal noise spectrum of an AFM cantilever

The first method of calibration can cause the problem of damage to the tip as an arbitrary penetration distance is mentioned, which can generate a force that is large enough for the tip to be damaged. However, the second method is non-contact and causes no such damage to the tip [34]. Due to economic reasons, the second method of calibration is used for this study.

CHAPTER 4

SAMPLE DESCRIPTIONS

All the samples used in this study were supplied by Army Research Lab via Solvus Global. The samples were cold sprayed on a metal substrate.

4.1 Multi-spray samples

All the samples under this category were cold-sprayed multiple times on the substrate. A graphical representation of this process is shown in Figure 27.

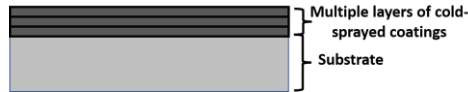


Figure 27: Graphical depiction of multiple pass cold-spray process

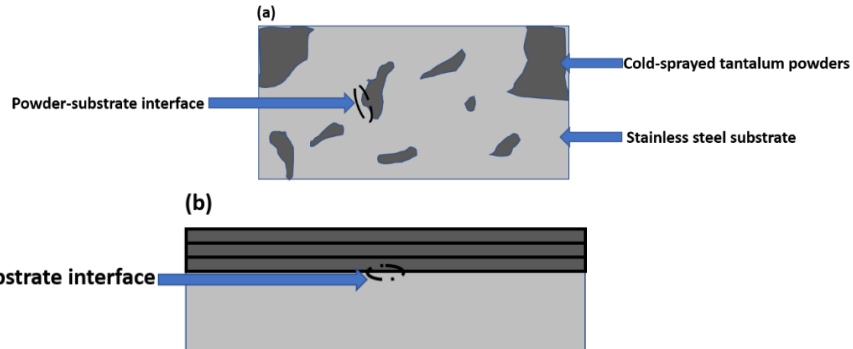


Figure 28: Graphical representation of Tantalum-stainless steel samples (a) top cross-section (b) vertical cross-section

4.1.1 Tantalum powder-stainless steel substrate sample (Ta-SS)

In this type of samples, conventional tantalum powders were sprayed on stainless steel substrates. The samples were polished on both the top surface and the vertical cross-section.

4.1.2 Low-hydrogen treated Tantalum powder-stainless steel substrate samples (LTa-SS)

In this type of samples, the tantalum powders were first treated in a low-hydrogen environment. They were then sprayed on the stainless steel substrates. This type of samples

was also polished on both the top surface and the vertical cross-section. Figure 28 graphically shows the samples in the above category.

4.2 Single-spray sample

This type of sample was sprayed for only one layer on an aluminium substrate. The powder being conventional Tantalum. They were processed in a nitrogen environment. Figure 29(a) shows a single-pass sample. The sample was not polished and the top surface was investigated. Figure 29(b) shows the surface investigated.

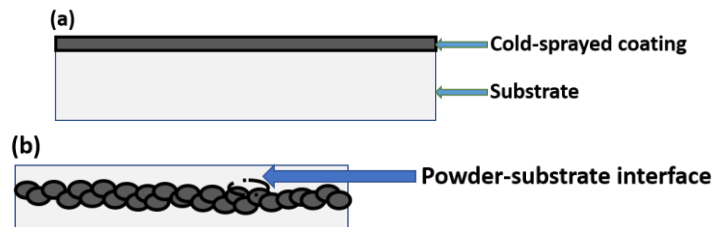


Figure 29: (a) Graphical representation of single-spray cold-sprayed coating (b) interface region investigated

CHAPTER 5

LOCAL VARIATIONS IN YOUNG'S MODULUS DUE TO TOPOGRAPHIC AND OXIDATION CHANGES

5.1 Topographic changes

5.1.1 Background and motivation

It is mentioned in section 2.3 that mapping using an atomic force microscope is a site-specific process. Therefore, it is quite dependent on the properties of the sample at that specific site. Figure 23 and 24 shows how the change in position of the z-piezo depends on the topography of the sample. Figure 30 is a summary of the process which determines the local modulus mapped. This, in turn, affects the Young's modulus measured. Since the work focuses on investigating local Young's modulus variations, it is quite essential to discuss the topography features influencing this process.

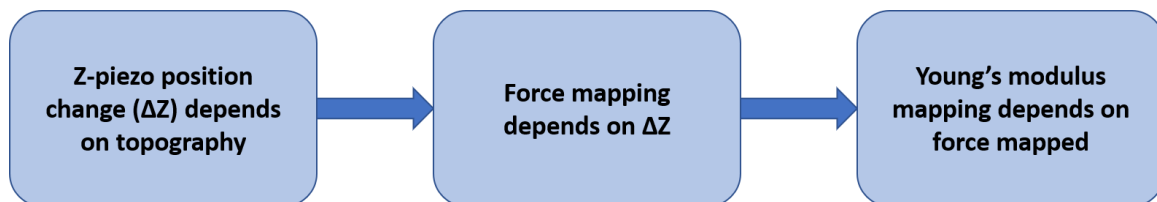


Figure 30: Process of mapping of local Young's modulus

5.1.2 Variations due to tip wear

The tip surface can be worn due to repeated usage-the topography changes as a result of it. From Figure 30, change in z-piezo position depends on topography which ultimately leads to error in local modulus mapping. Figure 31 depicts the change in topography due to the worn-out tip.

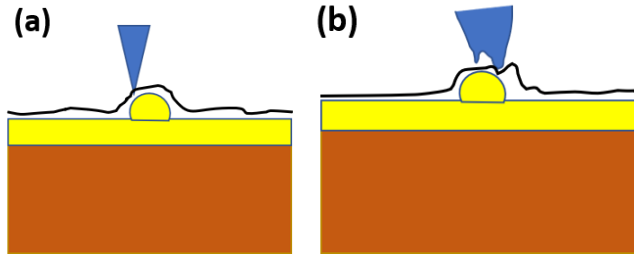


Figure 31: Difference in topography mapped due to tip wear (adapted from [47])

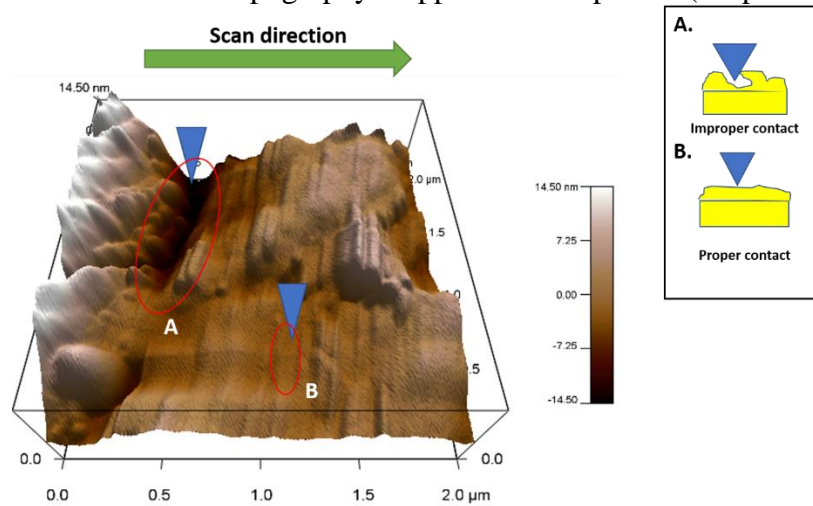


Figure 32: Improper volume of contact of tip and sample

5.1.3 Variations due to volume of the surface touched by the tip

Many times, due to the topography variations, there is improper contact between the tip and the sample surface, which affects the force applied and modulus mapped. Figure 32 depicts the phenomenon [47].

5.1.4. Variations due to sample particle deformation at the point of contact of the tip and sample

During the process where the cantilever tip impinges on the sample surface, it can cause some elastic or plastic deformation at that site. This causes hysteresis, which affects the tip deflection [48,49]. Referring to Figure 30, we can conclude that this process will ultimately influence the local modulus mapped. These processes can occur simultaneously or individually. The effects of these processes on the samples are discussed in this chapter.

5.1.5 Images obtained via AFM

The multi-spray samples were polished to obtain a uniform topography. The single spray samples were not polished as it would wear off the coated layer.

5.1.5.1 AFM tip calibration

The AFM cantilever tips were calibrated using the method described in section 3.2. This led to a reduction in tip damage. The Setpoint (force and cantilever deflection, which comes first) was given as input according to the calibrated data obtained.

5.1.5.2 Interpretation of the images

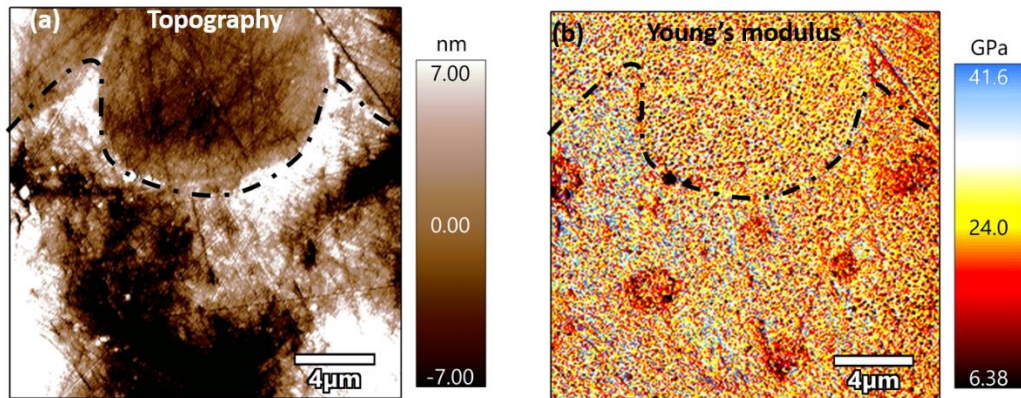


Figure 33: (a) Topography (b) local Young's modulus variations of Ta-SS vertical cross-section samples (black line shows the interface between coating and substrate)

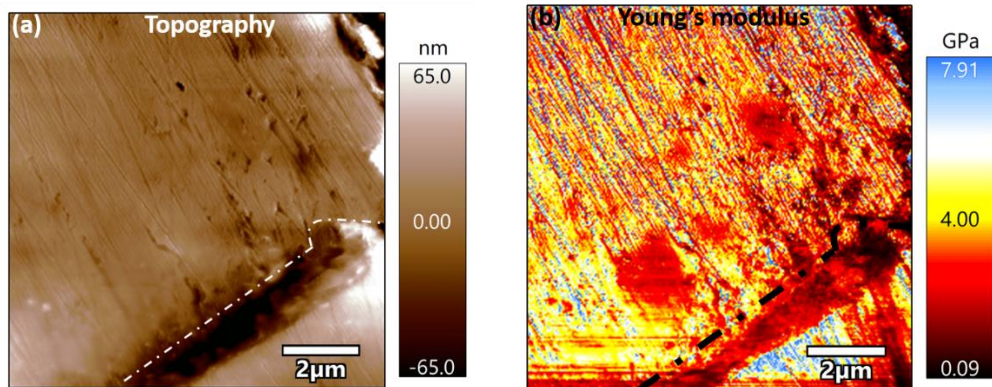


Figure 34: (a) Topography (b) local Young's modulus variation of LTa-SS vertical cross-section samples (white line in (a) and black line in (b) shows the interface of coating with substrate)

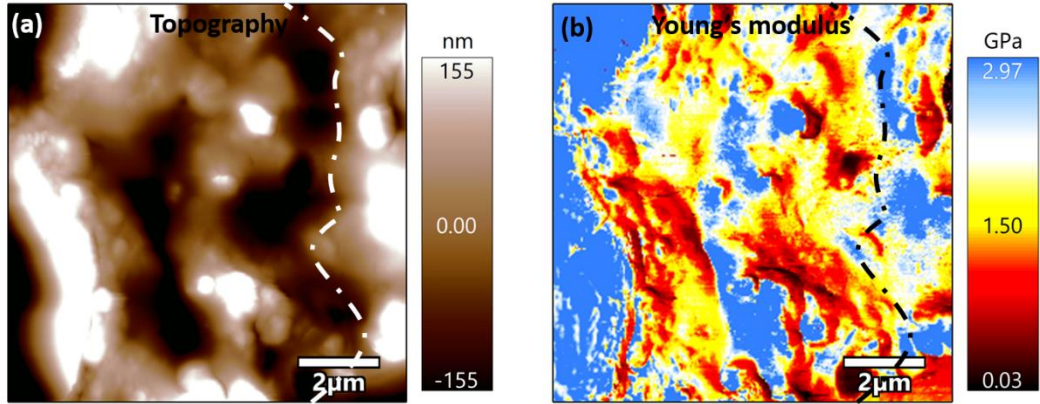


Figure 35: (a) Topography (b) Young's modulus variations in Ta-SS top interface (white line in (a) and black line in (b) indicates the interface between coating and substrate)

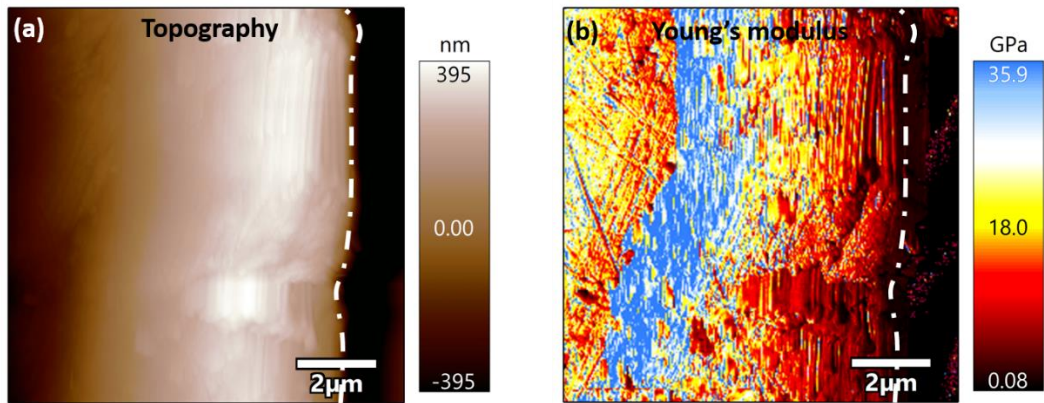


Figure 36: (a) Topography (b) Young's modulus variations in L-Ta-SS top interface (white line shows the interface between coating and substrate)

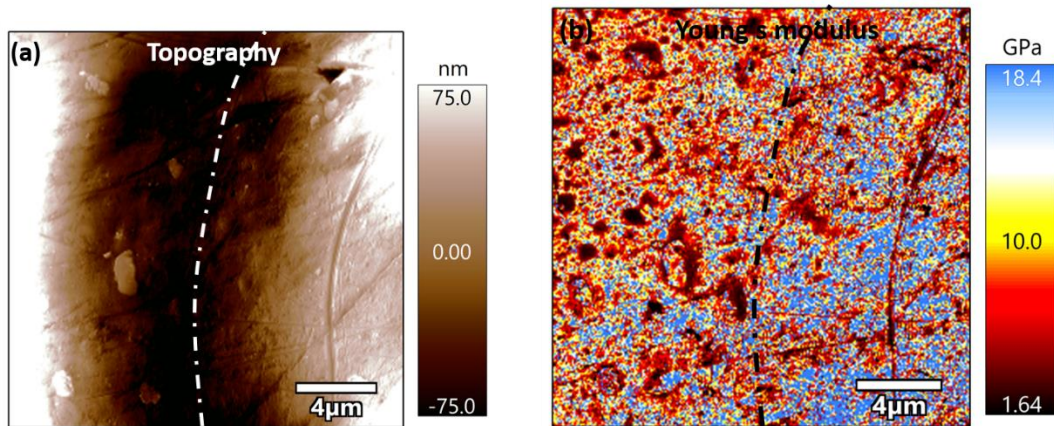


Figure 37: (a) Topography (b) Young's modulus variations in Ta-Al sample (white line in (a) and black line in (b) shows the interface)

Figure 33 shows the vertical cross-section of the conventional Tantalum-stainless steel (Ta-SS) sample. The dark regions in topography indicates some trough-like features that caused the tip to have improper contact with the sample (as mentioned in section 5.2). The

same can be said for figures 34-37. Overall, the variation in Young's modulus in the sample can be a result of the topography variations, which are mentioned in this chapter (sections 5.2, 5.3).

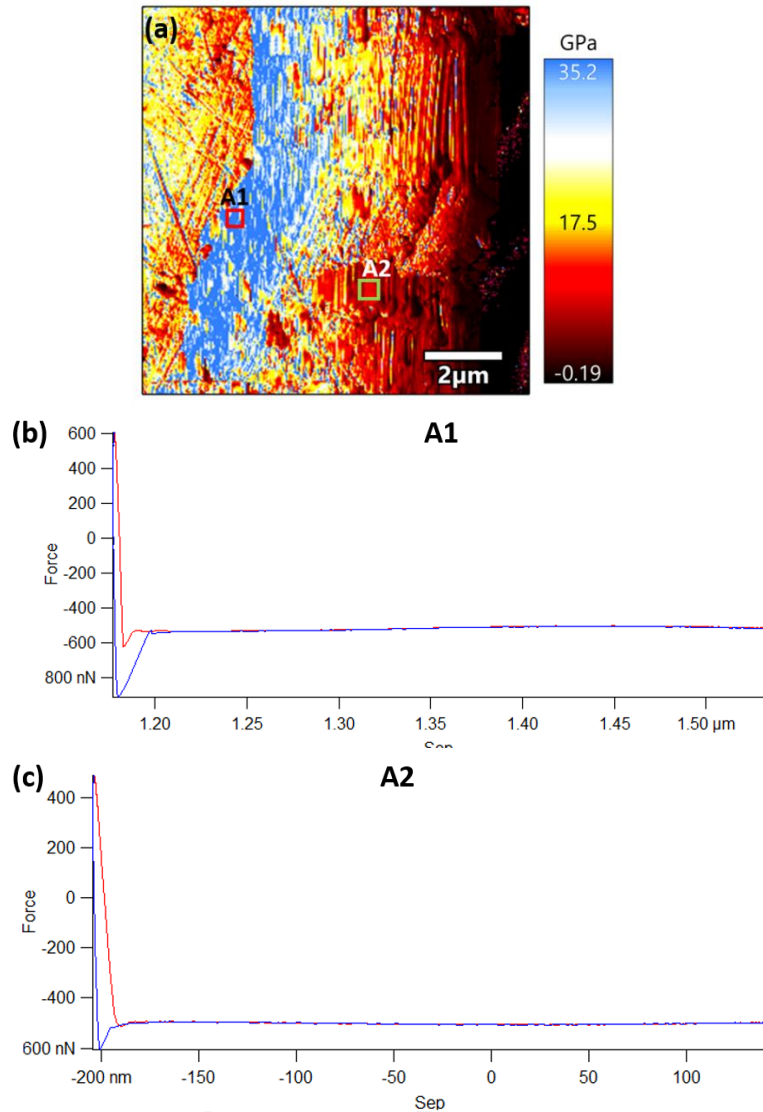


Figure 38: (a) Local modulus variation (b), (c) force-distance curves indicating local particle deformation of LTa-SS top section sample

Figure 38 shows the force-distance curve of the top section of LTa-SS sample. The variation in hysteresis in the two plots indicates local particle deformation in region A2, which affected the modulus mapped (section 5.3).

5.2 Oxidation changes

5.2.1 Background and motivation

It has been discussed in section 2.3, that minute traces of oxygen can be present in CS coatings. Furthermore, the oxide inclusions can result in a reduction in ductility, which can often not be removed by post – processing heat treatments[16]. It has been reported that tantalum can be cold – worked till 500°C, beyond which results in excessive oxidation[50].

Li et al.[51] has used finite element modeling to understand the widely accepted phenomenon of deformation of powder particles during particle deposition in CS. Figure 39 shows how an oxide film both at the substrate and particle can be disrupted during particle impact, thus permitting metallic bonding. However, some oxide debris remain. It has also been reported elsewhere that oxide inclusions at the interfaces inhibit bonding and lower the bond strength of the sprayed particles[52].

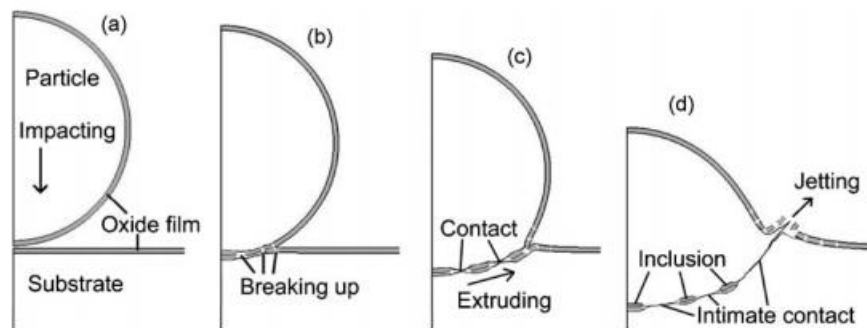


Figure 39: Schematic diagram of particle impact and bonding at the interface of sprayed particle and substrate interface[51]

The interface is the place where the first bond between CS particle and substrate takes place. It is where oxide can be present, and a study of the influence of oxide inclusions will give an idea of its effects on bonding.

There is also a difference in the bond energy between Ta-Ta atoms and Ta-O atoms, as one is a metal-metal and the other is a metal-nonmetal bond (Figure 40) [53].

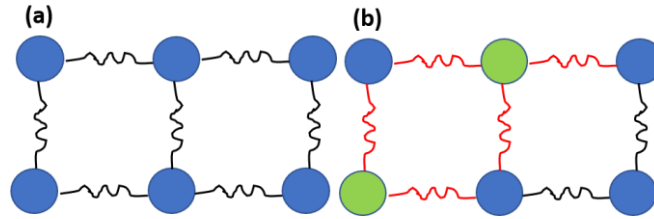


Figure 40: (a) Bond between Tantalum atoms (b) red lines show different bonds due to the presence of oxygen atoms

Young's modulus definition on the atomic scale is that it is the resistance to bond deformation. Thus, due to different bond energies, the presence of oxide causes local changes in the Young's modulus [54]. These local changes are discussed in the following chapter.

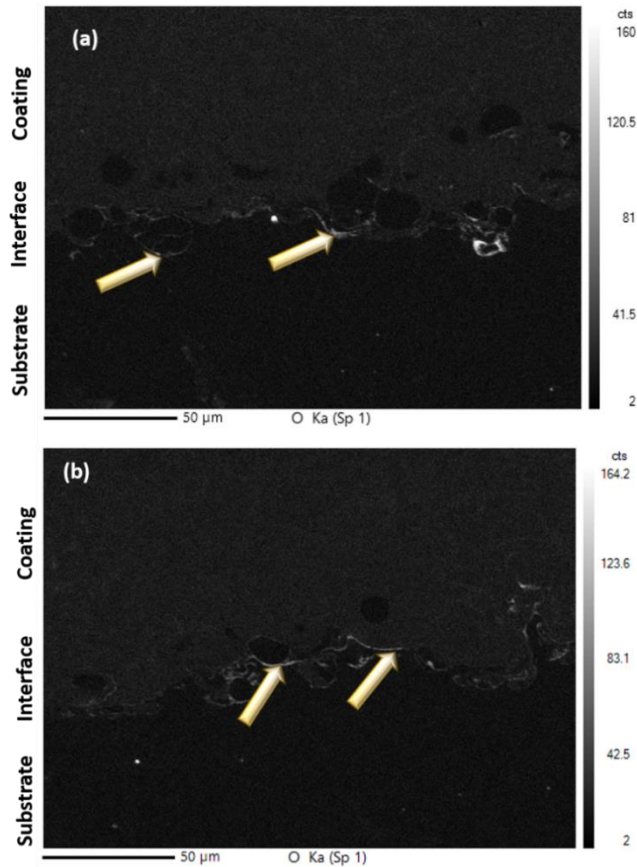


Figure 41: EPMA study showing oxide content at the coating-substrate interface (a) Ta-SS (b) L-Ta-SS vertical cross-section samples

5.2.2 Electron micro-probe analysis (EPMA) of Tantalum-stainless steel cross-section interface samples

EPMA was done on Ta-SS and LTa-SS samples using the X-ray dispersive wavelength spectroscopy (WDS) mode (Figure 41). The arrows point out the regions at the coating-substrate interface where the oxide content is high. The mapping shows there are very few high oxide sites in areas away from the interface.

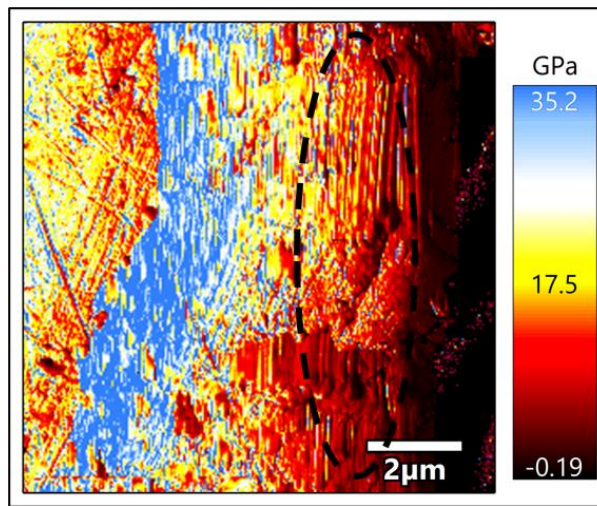


Figure 42: Local modulus changes along the interface of LTa-SS (black lines) can be due to the presence of oxides

5.2.3 Local modulus mapping using AFM

The samples described in the previous chapter were investigated for oxide content, and AFM tips were calibrated using the same method.

As Young's modulus is the resistance to bond deformation, oxide content influences it as it interrupts the bond energy (section 5.1). The forces between tip and surface also is influenced by this change in bond energy, which causes variations in the local modulus mapped (Figure 42).

CHAPTER 6

CONCLUSIONS

It can be concluded that AFM is a useful technique to map the local variations nanomechanical variations of any material. Its main advantage lies in its versatility in measuring the properties of any material. The scan area is divided into segments, where the AFM cantilever tip is interacted with the sample to give a force-distance curve. The local Young's modulus is calculated using this force-distance curve. Force-distance curves at various sections of the map region give the local variation of the modulus. It is a site-specific process, and factors such as sample properties and topography play a key role in shaping the AFM maps.

An important step before the start of any measurement using AFM is the calibration of the cantilever, which is used in measuring the properties. The variation in its angle (on which the force applied by it depends) is the main driving motivation behind calibration. The conventional calibration method is by contacting the tip of the cantilever with any hard, non-deformable substance with a pre-defined force applied and deflection. This gives a deflection vs. tip penetration depth curve; the inverse of the slope gives Inverse optical lever sensitivity (InvoLS), which is the sensitivity of the photodetector, which turns the deflection of the cantilever into a voltage signal. This work uses a non-contact method of calibrating the cantilever. The atomic force microscope used in this work uses a feature called "GetReal®" which calculates InvoLS using the thermal noise spectrum with

cantilever dimensions and drive frequency as the governing parameters. It shows the resonant frequency as the peak and also calculates the calibrated stiffness of the cantilever

The CS process has a lower operating temperature than conventional thermal spray techniques. This lowers the chances of high oxide and porosity content of cold-sprayed coatings. Evidence shows that oxide content in CS coatings cannot be completely eliminated. Oxide content disrupts the bonding between CS particles and hence causes changes in the mechanical properties. The interface between the CS coating and the substrate is the first place where the bonding process takes place. Therefore, it is crucial to study the bonding phenomenon at the interface. This work shows some preliminary evidence of oxide content at the interface using Electron micro probe analysis (EPMA). The local change in modulus can occur due to oxide, among the other processes described below.

As mentioned earlier, AFM is a site-specific process, and sample topography plays vital role in shaping its measurements. This work also investigates the effect of topography. As a contact-based mapping technique is used, tip wear is a problem. A worn-out tip causes an error in topography mapping of the sample, which ultimately leads to variations in nanomechanics. The contact between AFM cantilever tip and the sample determines the force applied using the contact mechanics model, the primary factor which determines the Young's modulus mapped. Local deformation of sample particles at the site of AFM cantilever tip contact causes hysteresis in the force-distance curve at that point. This causes errors in the cantilever deflection, ultimately leading to an error in the measurement of the local modulus.

CHAPTER 7

FUTURE WORK

The process of Atomic force microscopy (AFM) contact-based mapping can be done for other refractory metals, such as tungsten [55], or metals having refractory-like properties, such as Titanium [41]. A comparison of local nanomechanics at different sites can be made for various coatings.

Nanomechanics can also be studied using nanoindentation techniques. However, AFM has an edge to it as it is a non-destructive process and also, it's having a more precise scale of measurement [39]. It will be interesting to note the differences in nanomechanical measurement using AFM and some other nanoindentation techniques. The present work discussed how surface topography affects the nanomechanics of cold-sprayed coatings. A future effort can be in the area of the improvement of the topography [56]. A different metal polishing technique can also be applied in this case [57].

Variation in the cold-spray parameters can be an interesting study as it determines factors such as bonding between particles [6,7]. The present work states how bonding between particles influences their nanomechanical properties. Therefore, variation in cold-spray parameters will affect the nanomechanics of the sprayed region. The current work has theoretically mentioned how bonding energy is altered due to the presence of oxides. It'll be interesting to note the quantitative variation in the bond energy due to oxides using appropriate techniques [58].

The stiffness of the cantilever used in AFM is a major driving factor behind its nanomechanical measurements [43]. An important study will be the use of cantilevers with different stiffness and their effect on the local nanomechanical variations. AM-FM bimodal nanomechanical mapping is a technique that involves mapping without using force-distance curves. As this is a non-contact mode of mapping, it will cause significantly less damage to the tip [37].

BIBLIOGRAPHY

- [1] Yin, S., Chen, C., X. Suo, X., Lupoi, R., *Cold-Sprayed Metal Coatings with Nanostructure*, Thermal Spray Technology, 2018, 1-20
- [2] V. K. Champagne, *Introduction, The Cold Spray Materials Deposition Process: Fundamentals and Applications*, Elsevier Ltd., 2007, 1–7
- [3] da Silva, F., S., Cinca, N., Dosta, S., Cano, I. G., Guilemany, J., M., Benedetti, A., V., *Cold gas spray coatings: Basic principles, corrosion protection and applications*, Ectetica Quimica, 42(1), 2017, 9–32
- [4] M. F. Smith, *Comparing cold spray with thermal spray coating technologies*, *The Cold Spray Materials Deposition Process: Fundamentals and Applications*, Elsevier Ltd., 2007, pp. 43–61
- [5] Tejero-Martin, D., Rezvani Rad, M., McDonald, A., Hussain, T., *Beyond Traditional Coatings: A Review on Thermal-Sprayed Functional and Smart Coatings*, Journal of Thermal Spray Technology, 28, 2019, 598–644
- [6] M. Walker, *Microstructure and bonding mechanisms in cold spray coatings*, Materials Science and Technology, 34(17), 2018, 2057–2077
- [7] Schmidt, T., Gärtner, F., Assadi, H., Kreye, H., *Development of a generalized parameter window for cold spray deposition*, Acta Materialia, 54(3), 2006, 729–742
- [8] Hussain, T., McCartney, D., G., Shipway, P., H., Zhang, D., *Bonding mechanisms in cold spraying: The contributions of metallurgical and mechanical components*, Journal of Thermal Spray Technology, 18(3), 2009, 364–379
- [9] Rokni, M., R., Nutt, S., R., Widener, C., A., Champagne, V., K., Hrabe, R., H., *Review of Relationship Between Particle Deformation, Coating Microstructure, and Properties in High-Pressure Cold Spray*, Journal of Thermal Spray Technology, 26(6), 2017, 1308–1355
- [10] Li, C., J., Li, W., Y., Wang, Y., Y., Fukanuma, H., *Effect of Spray Angle on Deposition Characteristics in Cold Spraying*, Thermal Spray 2003: Advancing the Science and Applying the Technology (ASM International), 2003, 91-96
- [11] Yin, S., Suo, X., Su, J., Guo, Z., Liao, H., Wang, X., *Effects of Substrate Hardness and Spray Angle on the Deposition Behavior of Cold-Sprayed Ti Particles*, Journal of Thermal Spray Technology, 23, 2014, 76-83
- [12] Li, W., Y., Zhang, C., Guo, X., P., Zhang, G., Liao, H., L., Li, C., J., Coddet, C., *Effect of standoff distance on coating deposition characteristics in cold spraying*, Materials and Design, 29(2), 2008, 297–304

- [13] Cetin, O., Tazegul, O., Kayali, E., S., Effect of Parameters to the Coating Formation during Cold Spray Process, Proceedings of the 2nd World Congress on Mechanical, Chemical, and Material Engineering (MCM'16), 2016, MMME 140 1-7
- [14] Snead, L., L., Hoelzer, D., T., Rieth, M., Nemith, A., A., N., *Refractory Alloys: Vanadium, Niobium, Molybdenum, Tungsten*, Structural Alloys for Nuclear Energy Applications, 2019, 585–640
- [15] J. L. Johnson, D. F. Heaney, N. S. Myers, *Metal injection molding (MIM) of heavy alloys, refractory metals, and hardmetals*, *Handbook of Metal Injection Molding*, 2019, 535–573
- [16] Barnett, B., Trexler, M., Champagne, V., *Cold sprayed refractory metals for chrome reduction in gun barrel liners*, *International Journal of Refractory Metals and Hard Materials*, 53, 2015, 139–143
- [17] Yin, S., Cavaliere, P., Aldwell, B., Jenkins, R., Liao, H., Li, W., Lupoi, R., *Cold spray additive manufacturing and repair: Fundamentals and applications*, *Additive Manufacturing*, 21, 2018, 628-650
- [18] S. Kumar, M. Kumar, and N. Jindal, *Overview of cold spray coatings applications and comparisons: a critical review*, *World Journal of Engineering*, 17(1), 2020, 27–51
- [19] Ševeček, M., Gurgun, A., Seshadri, A., Che, Y., Wagih, M., Phillips, B., Champagne, V., Shirvan, K., *Development of Cr cold spray-coated fuel cladding with enhanced accident tolerance*, *Nuclear Engineering and Technology*, 50(2), 2018, 229–236
- [20] Widener, C., A., Ozdemir, O., C., Carter, M., *Structural repair using cold spray technology for enhanced sustainability of high value assets*, *Procedia Manufacturing*, 21, 2018, 361–368
- [21] V. K. Champagne, C. Widener, *Cold Spray Applications, Cold-Spray Coatings: Recent Trends and Future perspectives*, Springer Nature, 2018, 25–56
- [22] Binnig, G.K. (1988). *Atomic force microscope and method for imaging surfaces with atomic resolution* (US Patent No. 4,724,318) US Patent and Trademark Office <https://patents.google.com/patent/US4724318A/en>
- [23] Binnig, G., Quate, C., F., Gerber, Ch., *Atomic force microscope*, *Physical Review Letters*, 56(9), 1986, 930-934
- [24] Bhatt, P., M., Joshi, U., S., Shah, H., N., Brahmabhatt, P., K., *Low temperature atomic force microscopy-A review*, *IOSR Journal of Mechanical and Civil Engineering*, 2(3), 2012, 1-5

- [25] P. Eaton, P. West, *Atomic force microscopy*, Oxford University Press, 2018, 248
- [26] Babu, R., Singh, E., *Atomic force microscopy: A source of investigation in biomedicine*, International Journal of Electronic and Electrical Engineering, 7(1), 2014, 59-66
- [27] De Oliveira, R., R., L., Albuquerque, D., A., C., Cruz, T., G., S., Yamaji, F., M., Leite, F., L., *Measurement of the Nanoscale Roughness by Atomic Force Microscopy: Basic Principles and Applications*, Atomic Force Microscopy - Imaging, Measuring and Manipulating Surfaces at the Atomic Scale, 2012, 147-174
- [28] M. Yaseen, B. J. Cowsill, J. R. Lu, *Characterisation of biomedical coatings*, Coatings for Biomedical Applications, 2012, 176–220
- [29] Kontomaris, S., V., Malamou, A., *Hertz model or Oliver & Pharr analysis? Tutorial regarding AFM nanoindentation experiments on biological samples*, Materials Research Express, 7(3), 2020, 033001
- [30] Cárdenas-Pérez, S., Chanona-Pérez, J., J., Méndez-Méndez, J., V., Arzate-Vázquez, I., Hernández-Varela, J., D., Vera, N., G., *Recent advances in atomic force microscopy for assessing the nanomechanical properties of food materials*, Trends in Food Science & Technology, 87, 2019, 59–72
- [31] Garcia, R., *Nanomechanical mapping of soft materials with the atomic force microscope: methods, theory and applications*, Chemical Society Reviews, 5850, 2020, 5850-5882
- [32] Benaglia, S., Gisbert, V., G., Perrino, A., P., Amo, C., A., Garcia, R., *Fast and high-resolution mapping of elastic properties of biomolecules and polymers with bimodal AFM*, Nature Protocols, 13(12), 2018, 2890–2907
- [33] Chighizola, M., Puricelli, L., Bellon, L., Podestà, *Large colloidal probes for atomic force microscopy: fabrication and calibration issues*, Journal of Molecular Recognition, 34, 2021, 1-14
- [34] Higgins, M., J., Proksch, R., Sader, J., E., Polcik, M., Mc Endoo, S., Cleveland, J., P., Jarvis, S., P., *Noninvasive determination of optical lever sensitivity in atomic force microscopy*, Review of Scientific Instruments, 77, 2006, 013701
- [35] Kuznetsova, T., Zubar, T., Chizhik, S., Gilewicz, A., Lupicka, O., Warcholinski, B., *Surface Microstructure of Mo(C)N Coatings Investigated by AFM*, Journal of Materials Engineering and Performance, 25(12), 2016, 5450–5459
- [36] Benaglia, S., Amo, C., A., Garcia, R., *Fast, quantitative and high resolution mapping of viscoelastic properties with bimodal AFM*, Nanoscale, 11(32), 2019, 15289–15297

- [37] Kocun, M., Labuda, A., Meinhold, W., Revenko, I., Proksch, R., *Fast, High Resolution, and Wide Modulus Range Nanomechanical Mapping with Bimodal Tapping Mode*, ACS Nano, 11(10), 2017, 10097–10105
- [38] L. L. Snead, D. T. Hoelzer, M. Rieth, A. A. N. Nemith, *Refractory Alloys: Vanadium, Niobium, Molybdenum, Tungsten, Structural Alloys for Nuclear Energy Applications*, 2019, 585–640
- [39] Kong, L., Hadavimoghaddam, F., Li, C., Liu, K., Liu, B., Semnani, A., Ostaddhassan, M., AFM vs. Nanoindentation: Nanomechanical properties of organic-rich Shale, Marine and Petroleum geology, 132, 2021, 105229
- [40] Sripada, J., V., S., N., Gallant, M., F., Saha, G., C., Singh, R., Kondas, J., *Tantalum Based High-Pressure Cold Spray Coatings on Stainless Steel Substrate*, Key Engineering Materials, 813, 2019, 429–434
- [41] Kim, K., Kuroda, S., Watanabe, M., Huang, R., Fukanuma, H., Katanoda, H., *Comparison of Oxidation and Microstructure of Warm-Sprayed and Cold-Sprayed Titanium Coatings*, Journal of Thermal Spray Technology, 21(3), 2011, 550-560
- [42] Li, C., Li, W., Liao, H., *Examination of the critical velocity for deposition of particles in cold spraying*, Journal of Thermal Spray Technology, 15(2), 2006, 212-222
- [43] Kim, S., Lee, Y., Lee, M., An, S., Cho, S., *Quantitative visualization of the Nanomechanical Young's Modulus of Soft Materials by Atomic Force microscopy*, Nanomaterials, 11, 2021, 1593
- [44] Bhushan, B., *Contact mechanics of rough surface in tribology: multiple asperity contact*, Tribology Letters, 4, 1998, 1-35
- [45] Thomas, G., Burnham, N., A., Camesano, T., A., Wen, Q., *Measuring the mechanical properties of living cells using atomic force microscopy*, Journal of visualized experiments, 76, 2013, 1-8
- [46] <https://lsa.umich.edu/content/dam/chem-assets/chem-docs/00-0018-01%20Standard%20AFM%20Modes.pdf>
- [47] Marinello, F., Carmignato, S., Voltan, A., Savio, E., De Chiffre, L., *Error sources in atomic force microscopy for dimensional measurements: Taxonomy and modeling*, Journal of manufacturing science and engineering, 132, 2010, 030903
- [48] Mizes, H., A., Loh, K., G., Miller, R., J., D., Ahuja, S., K., Grabowski, E., F., *Submicron probe of polymer adhesion with atomic force microscopy: dependance on topography and material inhomogeneities*, Applied physics letters, 59, 1991, 2901

- [49] Capella, B., Baschieri, P., Frediani, C., Miccoli, P., Ascoli, C., *Force distance curves by AFM*, IEEE Engineering in medicine and biology magazine, 16(2), 1997, 58-65
- [50] J. L. Johnson, *Annealing of Refractory Metals, Heat Treating of Nonferrous Alloys*, ASM Handbooks Online, 2016, 664-666
- [51] Li, W., Y., Gao, W., *Some aspects on 3D numerical modeling of high velocity impact of particles in cold spraying by explicit finite element analysis*, Applied Surface Science, 255(18) 2009. 7878-7892
- [52] Li, W., Y., Li, C., J., Liao, H., *Significant influence of particle surface oxidation on deposition efficiency, interface microstructure and adhesive strength of cold-sprayed copper coatings*, Applied Surface Science, 256(16), 2010, 4953–4958
- [53] L. Pauling, *The nature of the chemical bond and the structure of molecules and crystals: an introduction to modern structural chemistry*, Cornell University Press, 1960
- [54] Padmavathi, D., A., *Potential energy curves & material properties*, Materials sciences and applications, 2, 2011, 97-104
- [55] Cizek, J., Vilemova, M., Lukac, F., Koller, M., Kondas, J., Singh, R., *Cold sprayed tungsten armor for tokamak first wall*, Coatings, 9(12), 2019, 836
- [56] Melentiev, R., Yu, N., Lubineau, G., *Polymer metallization via cold spray additive manufacturing: A review of process control, coating qualities, and prospective applications*, Additive manufacturing, 48, 2021, 102459
- [57] Deng, T., Li, J., Zheng, Z., *Fundamental aspects and recent developments in metal surface polishing with energy beam irradiation*, International journal of machine tools and manufacture, 148, 2020, 103472
- [58] W. Plieth, *Structure and Bonding*, Electrochemistry for materials science, Elsevier Ltd., 2008, 27-69